Evolution of texture and dislocation distributions in high-ductile austenitic steel during deformation

Shigeo Sato[a)]
Institute for Materials Research, Tohoku University, Sendai 980-8577, Japan

Toshiki Yoshimura
Institute of Multidisciplinary Research for Advanced Materials, Tohoku University, Sendai 980-8577, Japan

Yohei Takahashi
Department of Research, Nissan Arc, Ltd., Yokosuka 237-0061, Japan

Nao Yamada
Anton Paar Japan K.K., Shinagawa-Ku, Tokyo 140-0001, Japan

Kazuaki Wagatsuma
Institute for Materials Research, Tohoku University, Sendai 980-8577, Japan

Shigeru Suzuki
Institute of Multidisciplinary Research for Advanced Materials, Tohoku University, Sendai 980-8577, Japan

(Received 19 January 2011; accepted 23 February 2011)

The microstructural evolution of Fe–Mn–C austenitic steels, which exhibit outstanding high-ductile deformation in their plastic regions, was characterized by line-profile and texture analyses. The convolutional multiple whole profile fitting procedure was used for a line-profile analysis of $2\theta-\theta$ diffraction data to evaluate variations of crystallite size, dislocation density, and dislocation arrangement. A substantial refinement of the crystallite size proceeded at an early deformation stage. In addition, the dislocation density increased with an increase in the tensile strain. Texture evolution was characterized by the analysis of orientation distribution functions. Three texture components grew with an increase in the tensile strain. According to the pole figure describing the full width at half maximum (FWHM) distribution of the 220 reflection, the nontextured grains had more microstructural defects than the textured grains. To evaluate the microstructural defects in detail, the 220 reflection observed at each texture orientation was analyzed by the single-line-profile method. The crystallite size and dislocation density were almost comparable, irrespective of the kind of texture component. The crystallite size of the nontextured grains was also comparable to that of the textured grains, whereas the nontextured grains had a dislocation density several times that of the textured grains. [DOI: 10.1154/1.3582806]

Key words: line-profile analysis, texture analysis, dislocation, crystallite, two-dimensional detector

I. INTRODUCTION

Fe–Mn–C austenitic steels exhibit outstanding tensile elongation of more than 70% in their plastic regions. This mechanical property is attributed to a synergetic effect of twinning-induced plasticity and slip deformation. In particular, the slip deformation predominantly affects the texture formation during the plastic deformation. Thus, microstructural evolution during plastic deformation has been investigated intensively by transmission electron microscopy and scanning electron microscopy with electron backscattered diffraction. The results primarily showed a microscopic morphology of deformed grains and preferred orientations (Barbier *et al.*, 2009; Gutierrez-Urrutia *et al.*, 2010). However, the micrographs showed that the crystal lattice in severely deformed grains is significantly distorted by the presence of dislocations and that the distribution of lattice distortion is uneven, depending on grains, which in turn indicates uneven distribution of dislocations. As plastic deformation is associated with the magnitude of the Schmid factor, which is defined by the relationship between the loading and crystal directions, it is essential to evaluate whether dislocation distribution can depend on the orientation of the texture. However, few studies focusing on quantitative characterization of microstrain due to dislocations, particularly from viewpoints of the texture, have been conducted for austenitic steels.

X-ray diffraction (XRD) line-profile analysis has been used to characterize microstrain caused by dislocations. Suzuki *et al.* (2008) examined the heating recovery process for deformed high-Mn austenitic steels by analyzing the variation of the full width at half maximum (FWHM) values of diffraction peaks. They suggested that the relation between the phase transformation and dislocation behavior could be well explained by the XRD data. Moreover, dislocation density and size distribution of crystallites can be estimated by careful analysis of diffraction profiles by the modified Williamson–Hall and modified Warren–Averbach methods (Ungár and Borbely, 1996). In general, a number of diffraction peaks from grains oriented in multiple crystal directions are measured in the Bragg–Brentano ($2\theta-\theta$ scan) geometry

[a)]Author to whom correspondence should be addressed. Electronic mail: s.sato@imr.tohoku.ac.jp

for line-profile analysis. Consequently, the estimated dislocation density and crystallite size correspond to average values reflected over the entire sample.

In order to evaluate texture-dependent microstrain, line profiles need to be measured with texture measurements. Generally, peak intensities of a diffraction peak are obtained through an XRD texture measurement by fixing a detector at a certain scattering angle. On the other hand, recent developments of a two-dimensional (2D) detector with a high angular resolution have facilitated estimation of line profiles through texture measurements. It is then possible to superimpose the line-profile information on the pole figure obtained by the texture measurement. By analyzing the line profiles that depend on the texture orientation, we can estimate the microstrain distribution according to textured components.

In this study, the microstructural evolution of a high-ductile Fe–Mn–C alloy is investigated by the XRD method. First, the variation in dislocation density and crystallite size with progression of plastic deformation is evaluated by using line profiles obtained from conventional XRD measurements. Second, texture analysis combined with single-line-profile analysis is carried out to analyze the dependence of dislocation distribution on the crystal orientation of grains. It should be mentioned that a single-line-profile analysis is not a strict method to decompose microstructural parameters of crystallite size and microstrain due to its simple analytical procedure. Nevertheless, we applied this method to show the possibility that the line-profile analysis based on texture analysis is able to offer a new insight into characteristics of deformed microstructures.

II. EXPERIMENTAL

The alloy used in this study was Fe–Mn (24.6)–C (0.59 mass %) austenitic steel. The master ingot of the alloy was prepared in a high-frequency induction furnace. The ingot was hot-forged and rolled after soaking at 1173 K to homogenize the composition and microstructure. Sheet samples with 1 mm gauge width, 10 mm gauge length, and 0.3 mm thickness were cut from the ingot and then were electropolished for a tensile test. The shaped samples were annealed at 1223 K for 1800 s in a vacuum. The rupture strain of this alloy was determined by a tensile test to be approximately 70%. Samples that were deformed by different amounts of nominal tensile strain—10%, 20%, 40%, and 60%—were used for XRD measurements.

The XRD measurement for the line-profile analysis was performed using a conventional X-ray diffractometer (D8 ADVANCE, Bruker AXS). Diffraction profiles were measured using Cu $K\alpha$ radiation in the Bragg–Brentano ($2\theta - \theta$) geometry. Instrumental line broadening was defined with diffraction profiles of the standard reference material LaB_6 marketed by National Institute of Standard and Technology (NIST). The convolutional multiple whole profile (CMWP) software (Ribarik *et al.*, 2004) was used for estimating the dislocation density and crystallite size.

The texture analysis of 111-, 200-, and 220-pole figures from the face-centered cubic crystal of the austenitic sample was carried out using an X-ray diffractometer (D8 DISCOVER, Bruker AXS), and the single-line analysis of the 220 reflection was carried out. The incident X-ray beam of monochromated Cr $K\alpha$ was collimated to a diameter of 0.3 mm, and diffracted X-rays were collected with a 2D detector equipped with the diffractometer. The distance between the sample and the detector plane was set to 150 mm. The experimental data were processed to analyze the orientation distribution function (ODF) using MTEX software (Hielscher and Schaeben, 2008). In addition, the de Keijser method (de Keijser *et al.*, 1982; Harjo *et al.*, 2001) was used for the single-line-profile analysis performed for estimating crystallite size and microstrain. In this analytical procedure, a line profile is fitted by the convolution of Gauss and Lorentz functions, which are reflective of microstrain ($\langle \xi^2 \rangle^{1/2}$) and crystallite size ($D$) and, respectively, with the following equations:

$$D = \frac{\lambda}{\beta_L \cdot \cos\theta}, \tag{1}$$

$$\langle \xi^2 \rangle^{1/2} = \left(\frac{2}{\pi}\right)^{1/2} \cdot \frac{\beta_G d_{hkl}}{2}, \tag{2}$$

where β_G and β_L are the parameters representing the breadths of the Gauss and Lorentz functions, respectively. However, it is rather crude to assign the Gauss and Lorentz parts to these microstructural parameters. Accordingly, the single-line-profile analysis does not consistently lead to exact values. Therefore, the microstructural parameters obtained by the single-line analysis are referred just to characterize microstructural habit depending on the texture.

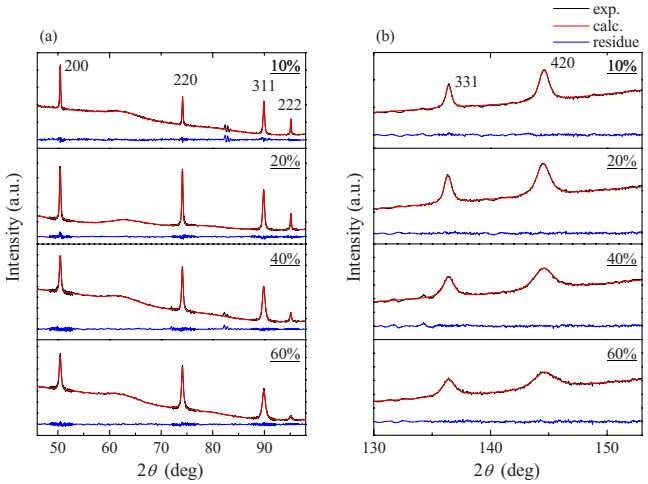

Figure 1. (Color online) Measured and fitted XRD profiles of middle-angle (a) and high-angle (b) parts for Fe–Mn–C austenitic steel at different deformation levels.

III. RESULTS AND DISCUSSION

A. Line-profile analysis using $2\theta - \theta$ diffraction data

Figure 1 shows the measured and fitted XRD patterns of the deformed Fe–Mn–C samples. The theoretical profiles were well fitted to the experimental ones. In this simulation, the 400 reflection was excluded from the fitting procedure because the intensity of this 400 reflection is considerably weak. In addition, the 111 reflection was also excluded from the fitting procedure because of the following reason. The

https://doi.org/10.1154/1.3582806 Published online by Cambridge University Press

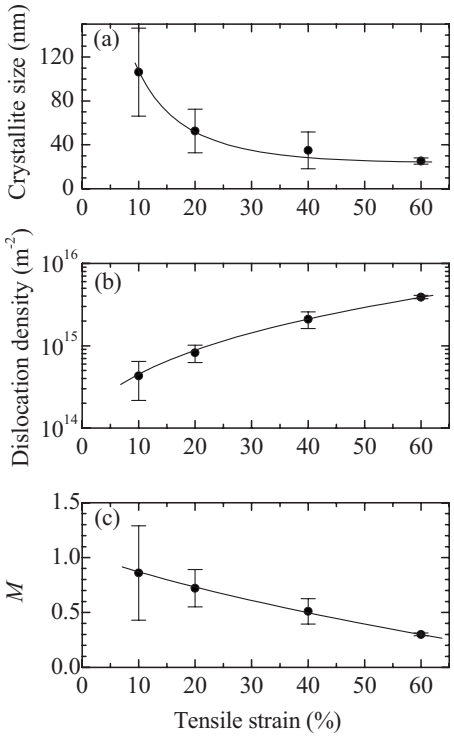

Figure 2. Variations of crystallite size (a), dislocation density (b), and dislocation arrangement parameter (c) of Fe–Mn–C steel with an increase in tensile strain.

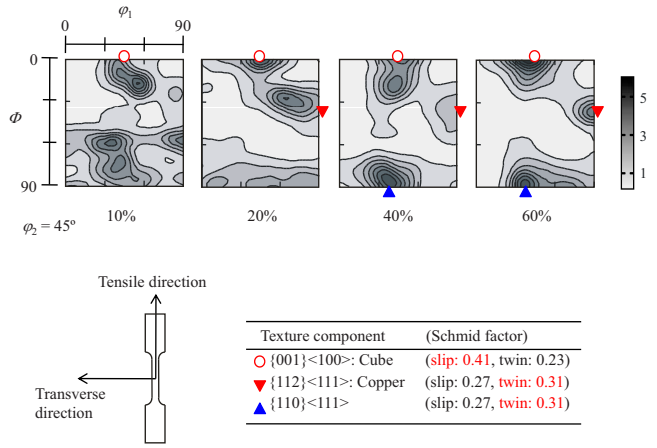

Figure 3. (Color online) ODF sections (φ_2=45°) of the Fe–Mn–C austenitic steel at different tensile strain levels. The Schmid factors of slip and twin deformations for the main texture components are also described.

111 reflection is prone to being insensitive to microstructural defects owing to its low scattering angle and the orientation relation between the Burgers vector and the scattering vector. Consequently, the breadth of the 111 reflection was almost comparable to that of the standard LaB_6 diffraction, especially for a low-strained sample. For example, the FWHM of the 111 reflection for a 10% strained sample is 0.071°, while that of the corresponding LaB_6 diffraction is 0.041°. The difference between these two FWHM values is only 0.03°. Moreover, the standard LaB_6 diffraction can be slightly broadened because of the marginal surface roughness and sample-transparency effects, resulting in the overestimation of the instrumental broadening. For example, 10 μm roughness on a sample surface increases FWHM by about 0.004° for the 111 reflection in our goniometer radius of 300 mm. Whereas the overestimation of the instrumental broadening is small, the effect is not negligible for a slightly broadened line profile. Since the 111 reflection have a rather strong effect on the crystallite size estimation owing to its low scattering angle and a low contrast factor for dislocations, the overestimation of the instrumental broadening for the 111 reflection caused poor convergence in estimating crystallite parameters. To reduce this influence, the diffraction peaks with Miller indices higher than the 111 reflection, which have a FWHM several times that of LaB_6 diffraction peaks, were used for the fitting procedure.

The estimated surface-weighted crystallite size as a function of the tensile strain is shown in Figure 2(a). The crystallite size decreases substantially up to an early deformation stage of 20% tensile strain, while the crystallite size decreases with further deformation. Such refinement is likely to contribute to the promotion of deformability of the Fe–Mn–C steel by reducing the unit volume for the deformation.

Figure 2(b) shows the variation of dislocation density with the tensile strain. A high density of dislocations is introduced even at an initial deformation of 10% tensile strain, and the dislocation density (ρ) reaches approximately 4×10^{15} m^{-2} at a near-rupture strain (60%). The variation of the dislocation arrangement parameter, M ($=R_e\sqrt{\rho}$, R_e: effective outer cut off radius), is shown in Figure 2(c). The M value decreases with an increase in the tensile strain, indicating that the dipole character of the dislocations and the screening of the displacement field are enhanced by the increase in the tensile strain. The screening effect of the dislocations can be brought about by the development of a cell wall and/or a small angle boundary, which are formed by peculiar arrangements of the dislocations. The decrease in the M value at the early deformation stage is likely to contribute to the development of these boundaries, resulting in a significant decrease in the crystallite size, as shown in Figure 2(a). It should be noted that the variation in the crystallite size diminishes beyond 20% tensile strain while the M value continues to decrease with the increasing tensile strain. This inconsistent phenomenon can be explained by the preferential formation of dislocation dipoles in crystallite domains because such dislocation dipoles do not affect the crystallite size. The property of high strain hardening, which is a characteristic of high-Mn austenitic steels (Barbier *et al.*, 2009), is likely to be associated with this preferential dipole formation.

B. Single-line-profile analysis based on texture measurement

Texture evolution along the tensile direction was analyzed using 111, 200, and 220 reflections. The ODF sections with φ_2=45° at different strain levels are shown in Figure 3. The texture components are described according to the $\{hkl\}\langle uvw\rangle$ notation. $\{hkl\}$ denotes the plane direction that is parallel to the normal direction of a sample surface and $\langle uvw\rangle$ denotes the direction parallel to the tensile direction. The evolution of the ODFs is characterized by three distinct texture components: $\{001\}\langle100\rangle$, $\{112\}\langle111\rangle$—which are

https://doi.org/10.1154/1.3582806 Published online by Cambridge University Press

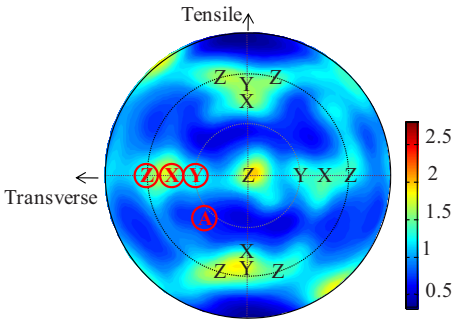

Figure 4. (Color online) Complete {110} pole figure of Fe–Mn–C austenitic steel at a nominal strain of 60%. The variables X, Y, Z, and A denote the cube, copper, {110}⟨111⟩, and nontexture components, respectively.

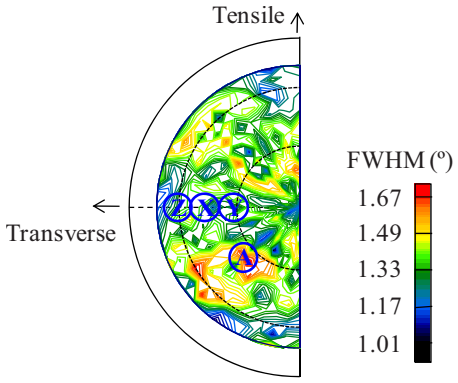

Figure 5. (Color online) Pole figure describing the 220 reflection FWHM of the Fe–Mn–C austenitic steel at a nominal strain of 60%. The variables X, Y, Z, and A denote the cube, copper, {110}⟨111⟩, and nontexture components, respectively.

generally described as cube and copper, respectively—and {110}⟨111⟩. These three texture components are dominant mainly at the near-rupture strain of 60%. The Schmid factors for slip and twinning deformations for these texture components are listed in the table in Figure 3. According to the Schmid factors, slip deformation can occur preferentially in the cube component, and twinning deformation can occur in the copper and {110}⟨111⟩ components. To investigate the dependence of crystallite size and microstrain on these different types of deformabilities, the single-line-profile analysis was carried out for each texture component.

Figure 4 shows the {110} complete pole figures at the nominal strain of 60%. Based on the ODF section in Figure 3, the cube, copper, and {110}⟨111⟩ components, which are denoted by the variables X, Y, and Z, respectively, can be individually assigned in Figure 4. The blue region in Figure 4 corresponds to a non-texture region. The pole figure describing the FWHM of the 220 reflection of austenitic steel at a 60% strain is shown in Figure 5. The FWHM of the 220 reflection of the corresponding nontexture region is larger than that of the texture region. This indicates that the nontextured grains have larger microstrain and/or smaller crystallite size than the textured grains. To estimate the distribution of the microstrain and crystallite size quantitatively, the line profiles of the 220 reflection ($2\theta \approx 127°$) at the orientations of the encircled X, Y, Z, and A marks in Figure 4 were analyzed by the de Keijser method (de Keijser *et al.*, 1982). The encircled A in Figure 4 represents the nontexture component. The 311 reflection of LaB_6 ($2\theta \approx 132°$) was measured for the instrumental line profiles at the equivalent geometry of the X, Y, Z, and A positions. The breadths of the Gauss and Lorentz parts for the observed, instrumental, and physical line profiles are summarized in Table I. The de Keijser method requires the breadth of an instrumental line profile to be sufficiently smaller than that of an observed line profile so that Gauss and Lorentz parts of a physical line profile can be estimated with high accuracy. As can be seen in Table I, the breadths of the observed line profiles were several times those of the corresponding instrumental line profiles. This indicates that the present diffractometer setup, which consists of the point-shaped (ϕ0.3 mm) incident beam and the 2D detector, is applicable to the line-profile analysis of the de Keijser method. It should be mentioned that the errors shown in Table I are statistical one, and systematic errors are not comprised in the errors. Thus, the actual errors can be larger. Nevertheless, we can safely say that physical breadths of the Lorentz part for texture and nontexture components are almost comparable, and that the physical breadth of the Gauss part for the nontexture component is larger than those for the texture components.

The estimated crystallite size and microstrain for the texture and nontexture components are listed in Table I. The crystallite size is independent of the texture components. Moreover, the microstrain for the texture components of the cube, copper, and {110}⟨111⟩ is almost comparable. Thus,

TABLE I. Breadths of the Gauss (bG) and Lorentz (bL) parts for the observed, instrumental, and physical line profiles of the Fe–Mn–C austenitic steel at the nominal strain of 60%. The estimated crystallite size (D) and microstrain ($\langle \xi^2 \rangle^{1/2}$) for texture and nontexture components are also summarized.

Texture component		Breadth (deg) Observed	Instrumental	Physical	D (nm)	$\langle \xi^2 \rangle^{1/2}$ (%)
	β_G	0.52 ± 0.03	0.11 ± 0.01	0.51 ± 0.03		
{001}⟨100⟩ cube	β_L	1.07 ± 0.02	0.12 ± 0.01	0.91 ± 0.03	36 ± 2	0.101 ± 0.006
	β_G	0.49 ± 0.03	0.09 ± 0.02	0.48 ± 0.03		
{112}⟨111⟩ copper	β_L	1.04 ± 0.02	0.18 ± 0.01	0.88 ± 0.03	37 ± 2	0.094 ± 0.007
	β_G	0.54 ± 0.03	0.10 ± 0.01	0.54 ± 0.03		
{110}⟨111⟩	β_L	1.12 ± 0.02	0.18 ± 0.01	0.94 ± 0.03	34 ± 1	0.106 ± 0.005
	β_G	1.09 ± 0.04	0.09 ± 0.02	1.08 ± 0.05		
Nontexture	β_L	1.12 ± 0.04	0.18 ± 0.01	0.95 ± 0.05	34 ± 2	0.215 ± 0.008

https://doi.org/10.1154/1.3582806 Published online by Cambridge University Press

the difference in the Schmid factors of these texture components does not have a significant influence on the microstructural defects. This indicates that the quantities of these microstructural defects do not reflect the deformability based on Schmid factors. The microstrain of the nontextured grains is about twice those of the textured grains. Since dislocation density is proportional to the square of the microstrain (Williamson and Smallman, 1956), the dislocation density of the nontextured grains is about four times those of the textured grains. One possible explanation for this dislocation distribution is that grains surrounding the nontextured grains would restrict the slip deformation of the nontextured grains. As a result, dislocations in the nontextured grains could not be annihilated. Hence, dislocations would accumulate in the nontextured grains.

IV. CONCLUSION

The Fe–Mn (24.6)–C (0.59 mass %) austenitic steel, which exhibits high-ductile deformability, was elongated by a tensile test. The characteristics of texture evolution and microstructural defects were evaluated by XRD. The main results obtained are summarized as follows:

(1) The refinement of crystallite size occurs mainly up to the early deformation stage (~20% strain), and the refined crystallites reach a size of several tens of nanometers. Such crystallite refinement is likely to contribute to the promotion of deformability of the Fe–Mn–C steel by reducing the unit volume for the deformation. In contrast, the dislocation density increases continuously with an increase in the tensile strain. The dipole character of dislocations is also enhanced with the increase in dislocations, which bring about a high strain-hardening feature of Fe–Mn–C austenitic steels.
(2) Three kinds of texture components are formed with a tensile deformation. Although the deformabilities expected from their Schmid factors are different from each other, no significant difference is observed in their crystallite size and dislocation density. However, the nontextured grains have much higher dislocation density than the textured grains. We deduce that dislocations in the nontextured grains accumulate because the deformation of nontextured grains would be probably restricted by the surrounding grains.

ACKNOWLEDGMENT

This research was partially supported by the Ministry of Education, Science, Sports and Culture, Japan, by a Grant-in-Aid for Young Scientists (B), Grant No. K022760572, 2010.

Barbier, D., Gey, N., Allain, S., Bozzolo, N., and Humbert, M. (**2009**). "Analysis of the tensile behavior of a TWIP steel based on the texture and microstructure evolutions," Mater. Sci. Eng., A **500**, 196–206.

de Keijser, Th. H., Langford, J. I., Mittemeijer, E. J., and Vogels, A. B. P. (**1982**). "Use of the Voigt function in a single-line method for the analysis of X-ray diffraction line broadening," J. Appl. Crystallogr. **15**, 308–314.

Gutierrez-Urrutia, I., Zaefferer, S., and Raabe, D. (**2010**). "The effect of grain size and grain orientation on deformation twinning in a Fe–22 wt.% Mn–0.6 wt.% C TWIP steel," Mater. Sci. Eng., A **527**, 3552–3560.

Harjo, S., Tomota, Y., Lukáš, P., Neov, D., Vrána, M., Mikula, P., and Ono, M. (**2001**). "In situ neutron diffraction study of $\alpha-\gamma$ Fe–Cr–Ni alloys under tensile deformation," Acta Mater. **49**, 2471–2479.

Hielscher, R., and Schaeben, H. (**2008**). "A novel pole figure inversion method: Specification of the *MTEX* algorithm," J. Appl. Crystallogr. **41**, 1024–1037.

Ribarik, G., Gubicza, J., and Ungar, T. (**2004**). "Correlation between strength and microstructure of ball-milled Al–Mg alloys determined by X-ray diffraction," Mater. Sci. Eng., A **387–389**, 343–347.

Suzuki, S., Senoo, S., Maruyama, T., and Shinoda, K. (**2008**). "Characteristic structural changes in stress-induced martensitic transformation and reverse transformation of a polycrystalline Fe–Mn–Si Alloy," Mater. Trans. **49**, 2755–2760.

Ungár, T., and Borbely, A. (**1996**). "The effect of dislocation contrast on x-ray line broadening: A new approach to line profile analysis," Appl. Phys. Lett. **69**, 3173–3175.

Williamson, G. K., and Smallman, R. E. (**1956**). "Dislocation densities in some annealed and cold-worked metals from measurements on the X-ray Debye-Scherrer spectrum," Philos. Mag. **1**, 34–36.